European Journal of Pharmaceutics and Biopharmaceutics 135 (2019) 25–35

Contents lists available at ScienceDirect

European Journal of Pharmaceutics and Biopharmaceutics

journal homepage: www.elsevier.com/locate/ejpb

Research paper

Redox-responsive prodrug-like PEGylated macrophotosensitizer nanoparticles for enhanced near-infrared imaging-guided photodynamic therapy

Zheng Ruan, Pan Yuan, Tuanwei Li, Youliang Tian, Quan Cheng, Lifeng Yan*

CAS Key Laboratory of Soft Matter Chemistry, Hefei National Laboratory for Physical Sciences at the Microscale, and Department of Chemical Physics, iCHEM, University of Science and Technology of China, Jinzai Road 96, Hefei 230026, Anhui, China

ARTICLE INFO

Keywords:
Photodynamic therapy
Photosensitizer
Near infrared (NIR)
Imaging-guided
Redox-responsive

ABSTRACT

Efficient delivery of hydrophobic photosensitizer (PS) into tumor cells is a key step for photodynamic therapy (PDT). Redox-responsive polymeric nanoparticles of amphiphilic macro-photosensitizer has designed and prepared as a prodrug-like pro-photosensitizer (pro-PS) for PDT. PEG works as the hydrophilic block and the near infrared (NIR) brominated BODIPY derivative (BDP) works as the hydrophobic PS, and they were linked *via* the disulfide bond as PEG-SS-BDP, which could be broken for drug release owing to the high GSH concentration inside tumor cells. The amphiphilic PEG-SS-BDP can be self-assembled into polymeric micelles with suitable size (about 110 nm), which benefits prolonged blood circulation and enhanced tumor accumulation confirmed by NIR fluorescent imaging *in vivo*. The higher efficiency of PEG-SS-BDP nanoparticles (PSSBDP NPs) than non-responsive PDT agent (PEG-BDP) with similar structure was confirmed by both *in vitro* and *in vivo* studies, suggesting the advantages of the redox-responsive pro-PS system for improving potential near infrared tumor imaging and photodynamic therapy.

1. Introduction

As an effective medical tool, photodynamic therapy (PDT) has been applied successfully for cancer treatment by inducing cell apoptosis or necrosis since it was first allowed for the treatment of carcinoma of urinary bladder in 1993 [1]. It is a non-invasive method using combination of photosensitizers (PSs) and molecule oxygen ($^3O_2$) under the excitation of appropriate wavelength light. PSs are activated by harmless light of specific wavelength, which could excite the PSs from the ground state to the triplet state [2–4]. The excited triplet can go through two kinds of reactions: (1) it can react with a substrate, such as a molecule or the cell membrane to form radicals by transferring the hydrogen atom (electron), and the radicals can interact with oxygen to generate oxygenated products (type I reaction); (2) the triplet can transfer its energy directly to oxygen, to form singlet oxygen - a highly reactive oxygen species (type II reaction) [1,5,6]. These reactive oxygen species (ROS) like oxygen radicals or singlet oxygen can induce the apoptosis of tumor cell, destroy the tumor vasculature, and activate an antitumor immune response [7,8].

Among the reported PDT photosensitizers, boron dipyrromethene (BODIPY) derivatives, which display outstanding characteristics including high molar extinction coefficients, high photostability, and ignorable dark toxicity, are recognized as promising photosensitizer for imaging-guided PDT [9–15]. Heavy atom effect by substituting with Br or I has been reported as a useful chemical method to improve inter-system crossing (ISC) in BODIPY chromophores for increasing the generation of singlet oxygen (type II) [16–18]. Nevertheless, most photosensitizers including BODIPYs have some shortcomings such as low solubility in aqueous solution and its non-specific distribution *in vivo* after intravenous injection, which significantly reducing the generation of ROS [12,19,20]. Even for some water-soluble PSs, the selective accumulation at tumor site is still not high enough for clinical application [21]. So the incorporation of photosensitizer into water-dispersible nanocarriers to form nanoparticles (NPs) is applied worldwide [22,23]. NPs with proper size (from 50 to 500 nm) are apt to accumulate in tumor tissues by passive targeting ability owing to the enhanced permeability and retention (EPR) effect [24–26].

After the nanoparticles get into tumor region, light permeation into tissues is the another hindrance for efficient PDT. Noticeably, near infrared (NIR) light (wavelength from 650 to 1000 nm), known as the “biological transparency window”, exhibits deeper penetration into tissues than UV or Vis light [20,27,28]. So it is important to shift the

* Corresponding author.
E-mail address: lfyan@ustc.edu.cn (L. Yan).

https://doi.org/10.1016/j.ejpb.2018.12.006
Received 1 September 2018; Received in revised form 5 December 2018; Accepted 10 December 2018
Available online 11 December 2018
0939-6411/

excitation wavelength of photosensitizer to NIR region for PDT at the deep-tissue level [29]. In our previous research, a novel brominated BODIPY was synthesized with high singlet oxygen quantum yield (Φ_Δ = 0.76) for efficient NIR PDT [30]. The photosensitizer we used here owns both high singlet oxygen quantum yield and NIR fluorescence, which could be applied for PDT and NIR bioimaging at the same time. Compared with other PDT agents, the Ce6 (Φ_Δ = 0.55) with bad photostability has too short stokes shift and difficult to be applied in fluorescence bioimaging. For IR780 (Φ_Δ = 0.127), IR783 (Φ_Δ = 0.007) or ICG (Φ_Δ = 0.008), their singlet oxygen quantum yields were not high enough for efficient PDT according to previous research [31].

When the photosensitizer in nanoparticles excited by illumination to generate singlet oxygen, the lifetime and diffusion radius of these $^1O_2$ are strongly limited inside cells. Within its short intracellular lifetime (about 3 μs), the apparent spatial field of $^1O_2$ activity will expected to have a spherical radius of 100 nm only, indicating a limited translational diffusion distance of $^1O_2$ within the cell [32]. Photosensitizer was always designed to release with biological stimuli-response so that sufficient $^1O_2$ could contact with organelle such as mitochondria then induce cell apoptosis [33–35]. Here, we have focused on the redox-responsive polymeric delivery systems [36–38]. Its basic principle is to utilize the different redox potentials between normal and tumor tissues. GSH/glutathione disulfide (GSSG) is reported as the richest redox couple in animal cells. Moreover, research in mice has proved that the tumor tissues showed more than 4-fold GSH concentration than normal tissues [39]. Among various reduction-responsive functional group in biomedical applications, disulfide linkages has been exploited and used extensively for constructing reduction-responsive drug delivery systems [40–43].

Here, we have designed a more efficient cargo delivery system for NIR imaging-guided PDT based on our previous research [30]. Redox-responsive macro-photosensitizer by combining hydrophilic poly (ethylene glycol) (PEG) and NHS-active brominated BODIPY (NHS-BDPBr) with a disulfide bond (named as PSSBDP, short for PEG-SS-BDP) has been synthesized. The amphiphilic macro-photosensitizer can be self-assembled as polymeric nanoparticles, which have suitable size for prolonged blood circulation and tumor accumulation *in vivo*. Especially, when the nanoparticles (pro-PS) get into the tumor cells, the disulfide linkage breaks for accelerated photosensitizer release because of the high GSH concentration (Scheme 1). The redox-responsive release leads shorter distance between BDP with organelle, which means the $^1O_2$ is more likely to diffuse to key organelle like mitochondria for cell killing. Compared with the PEG-BDP (PBDP) in our recent work, the redox-responsive PSSBDP here shows enhanced PDT efficiency.

2. Experimental

2.1. Materials

All solvents and reagents used were purchased from Sinoreagent Corporation, J&K (China) and Aladdin Corporation (China). Dimethyl sulfoxide (DMSO), dichloromethane (DCM) and N, N-dimethylformamide (DMF) were dehydrated by distilling with CaH_2. Deionized water was prepared by a Milli-Q System (Millipore, Bedford, MA, USA). Dialysis bags used here (cut off M_w = 3000/7000/10000) were obtained from Bomei Biotechnology Corporation. Cancer cells including HepG2 and EMT6 cells were originated from ATCC (American Type Culture Collection), which were incubated in Dulbecco's Modified Eagle's Medium (DMEM, Hyclone) with 10% fetal bovine serum (FBS, ExCell Bio, Shanghai, China) at 37 °C with 5% CO_2.

2.2. Characterization

^1H NMR spectra were recorded by a Bruker AC 400 or 300 spectrometer in chloroform-*d* ($CDCl_3$) or dimethyl sulfoxide-d_6 (DMSO-d_6). The molecular weight distribution (M_w/M_n) was measured by gel permeation chromatography (GPC) with a refractive index detector (RID-10A, Shimadzu) and a fluorescence detector (FLD, Shimadzu), using N, N-dimethylformamide (DMF) as eluent. A Malvern Zetasizer Nano ZS90 machine containing a He–Ne laser was applied for dynamic light scattering (DLS) detection and transmission electron microscopy (TEM) observation was conducted with a JEOL-2010 microscope with an accelerating voltage of 200 kV. The optical properties mentioned here were measured with an F97pro fluorescence spectrophotometer (Shanghai Lengguang Industrial Co. Ltd) and an UV1700pc (Shanghai AuCy Scientific Instrument Co., Ltd) ultraviolet spectrophotometer.

2.3. Synthesis of PEG-NPC

MPEG2000-OH (4.0 g, 2.0 mmol) and pyridine (0.79 g, 10 mmol) in 40 mL of anhydrous DCM were added into a flame-dried flask. After vigorous stirring at 0 °C in argon (Ar), p-NPC (1.61 g, 8.0 mmol) in 20 mL DCM was added dropwise to the mixture. Then the mixture was kept continual stirring for another 24 h then precipitated in cold diethyl ether, followed by filtration and dried under vacuum (yield: 86%).

2.4. Synthesis of PEG-SS-NH_2

Under Ar atmosphere, cystamine·2HCl (0.81 g, 4.0 mmol,) and triethylamine (0.81 g, 8.0 mmol) dissolved in 20 mL of anhydrous DMSO was dropwise added to PEG-NPC (0.8 g, 0.4 mmol) in anhydrous DMSO. Then the mixture was stirred for 48 h at 30 °C, followed by dialysis against deionized water. The PEG-SS-NH_2 was obtained after lyophilization (yield: 84%).

2.5. Synthesis of NHS-BDPBr (BDP)

The design and synthesis of photosensitizer boron dipyrromethene (BODIPY) derivatives (NHS-BDPBr) was according to our previous work [30]. The synthesis route of NHS-BDPBr (BDP) were shown in Fig. S1.

2.6. Synthesis of the macro redox-sensitive photosensitizer

PEG-SS-NH_2 (200 mg, 0.10 mmol) and NHS-BDPBr (106 mg, 1.2 eq.) were mixed in 10 mL dry DMF for 72 h stirring at room temperature. Then the mixture were dialyzed against deionized water. Diethyl ether was used to wash the solid after lyophilization to obtain 263 mg PEG-SS-BDP (PSSBDP, yield 91%).

2.7. Preparation and characterization of no stimuli–responsive PBDP nanoparticles (PBDP NPs) and redox-sensitive PSSBDP nanoparticles (PSSBDP NPs)

The PBDP without stimuli–responsive was synthesized referring to our previous research. The PSSBDP was dissolved in 3 mL DMF for 10 min vigorous stirring, followed the addition of 12 mL deionized water for another 30 min stirring. Then the mixture was dialyzed against deionized water to yield the polymeric micelles PSSBDP nanoparticles (PSSBDP NPs).

The size distribution and redox-responsive behavior of PSSBDP NPs with or without glutathione (GSH) were measured by dynamic lighting scatter (DLS, Malvern Instrument, Zetasizer Nano series, ZS90) and transmission electron microscopy (TEM, a JEOL-2010 microscope with an accelerating voltage of 200 kV). All PSSBDP micelle solutions were passed through membrane filters (pore size, 0.45 μm, Millipore).

2.8. Redox sensitivity and photosensitizer release

To enhance the solubility of BDP, the release of BDP was conducted with PSSBDP NPs in PBS (2% tween 80) and reduction buffer (10 mM GSH, 2% tween 80). The instant content of the photosensitizer release was monitored at predominant time points by an F97pro fluorescence

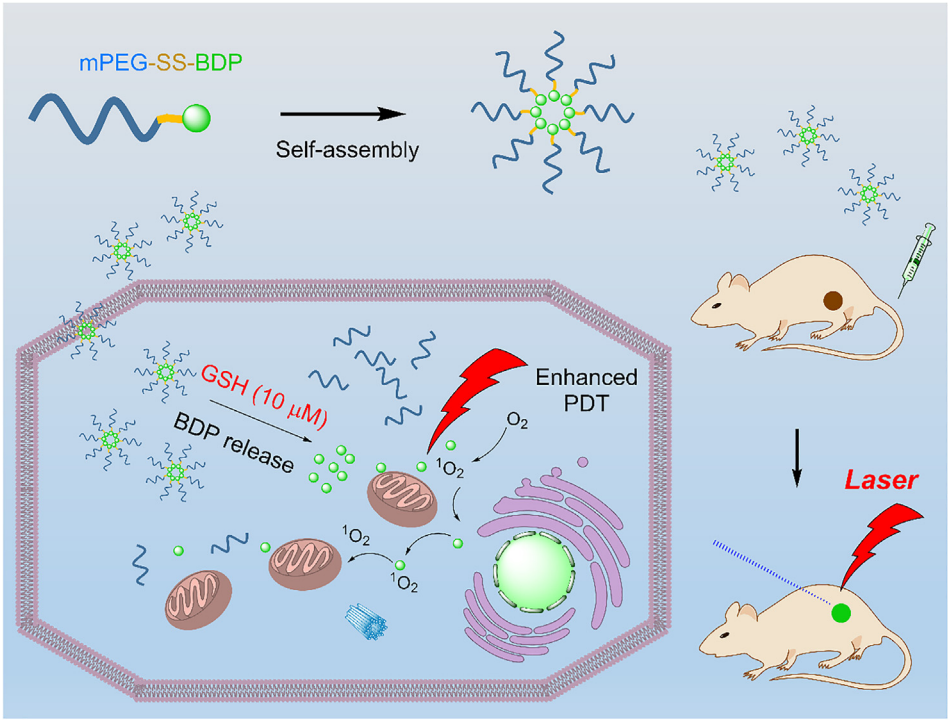

Scheme 1. Schematic illustration of the redox-responsive PEG-SS-BDP preparation and its release behavior in tumor cells for enhanced photodynamic therapy.

spectrophotometer (Shanghai Lengguang Industrial Co. Ltd) at an emission wavelength of 710 nm with an excitation wavelength of 670 nm.

2.9. Singlet oxygen generation of the macro redox-sensitive photosensitizer

1,3-diphenylisobenzofuran (DPBF) was applied as the ROS scavenger to measure the singlet oxygen generation ability. The absorption changes at 414 nm of DPBF was assigned to the consumption of singlet oxygen. The experiments were initially performed in DCM with methylene blue (MB) as reference (Φ_Δ = 0.57 in DCM), using irradiation of a 635 nm laser at 0.5 mW/cm^2. In brief, PSSBDP or MB (O.D ~ 0.5) with DPBF (O.D ~ 1.5) were mixed in DCM, followed by illumination at a 10 s interval.

2.10. Cytotoxicity evaluation in vitro

3000 HepG2 or EMT6 cells were seeded into each well (96-well plates). After 24 h, gradient concentration of PSSBDP or PBDP we synthesized before (from 0.001 mg/mL to 0.005 mg/mL) was added. A 660 nm laser output was applied for further illumination (20 mW/cm^2 for 10 min). At 24 h post-treatment, 0.02 mL methyl thiazolyl tetrazolium (MTT, 5 mg/mL) was added then replaced with 0.15 mL DMSO 4 h later. The mixture was shaken then measured with a Bio-rad iMark microplate reader for cell viability evaluation.

To observe the cytotoxicity directly, dead/live cell staining assays were conducted and performed with the fluorescence microscope. 10^5 HepG2 or EMT6 cells were incubated for 24 h in a 6-well plate. PSSBDP in medium at a concentration of 2 μM BDPI was added into the corresponding well and followed by irradiation 24 h later. Then a mixture of propidium iodide (PI, 0.100 mg/mL) and fluorescein diacetate (FDA, 0.010 mg/mL) in fresh medium was added to stain dead/live cells for further observation.

2.11. Cellular uptake

10^5 HepG2 or EMT6 cells was plated in 6-well plates per well in DMEM and each well was then incubated for 1 day. Afterwards, PSSBDP in DMEM (at concentration of 0.005 mg/mL BDP) replaced the medium for 24 h of incubation in darkness. Then each well was observed with an Olympus U-HGLGPS fluorescence microscope for cellular uptake evaluation.

2.12. Tumor model establishment

Protocols approved by the Animal Care and Use Committee in University of Science and Technology of China were applied for female BALB/c mice (5 weeks old, Beijing Vital River Laboratory Animal Technology Co., Ltd.) treatment. For establish the tumor model, EMT6 cells (500, 000 suspended in 100 μL PBS) were subcutaneously injected into the right side for NIR imaging, or both sides of the back for *in vivo* PDT performance. The mice were taken for further treatment when the volume of tumor grew to 100 mm^3 around.

2.13. In vivo accumulation of PSSBDP NPs

BALB/c mice with single tumor on the back were divided into three groups randomly (n = 2): mice treated with PBS as control, free BDP molecules and PSSBDP NPs, respectively. For experimental groups, free BDP molecule or PSSBDP NPs (at a same concentration of 5 mg/kg BDP) was intravenously injected to check their bio-distribution and accumulation at predetermined time points (2 h, 6 h, 12 h, 24 h and 48 h) by a Xenogen IVISs Lumina system (Caliper Life Sciences, USA). At 48 h post-treatment, mice were all sacrificed then tumors and main organs were collected for NIR fluorescent visualization.

Besides, the mice blood was collected for hemolytic potential assessment. After removing the plasm, PBS or PSSBDP was added into red blood cells for incubation together, and photographs were taken after centrifugation.

2.14. In vivo PDT

Tumor-bearing mice on both sides are randomly divided into four groups (n = 4): PBS, free BDP molecules, PBDP NPs without

stimuli–responsive property, PSSBDP NPs with redox-responsive property. With irradiation only for the tumors on the right side, different efficiency of PDT with or without laser could be directly observed by the growth of tumor volume. The mice in free BDP molecule group, PBDP NPs group or PSSBDP were given the same dosage (BDP concentration of 5 mg/kg). At 12 h post-treatment, the right tumor site was treated with illumination (660 nm laser, power density 25 mW/cm^2) for 20 min while no further irradiation on the left side. The injection and irradiation were only conducted with one repeat at the beginning.

Tumor volume and body weight were detailed every other day. The tumor volume was calculated with the equation: $V = (a \times b^2)/2$, in which *a* and *b* represent the maximum length and width of the tumors. 21 days later, mice were sacrificed for tumors collection. Then the tumors were photographed and their wet weight were recorded for further analysis.

For histological experiments, mice injected with PSSBDP was sacrificed, and the main organs were embedded by medium and fast frozen at −70 °C, sectioned into thin slices, stained with the hematoxylin and eosin (H&E) stain method, and observed by microscopy.

2.15. Statistical analysis

To measure diversity in different groups by mean, statistical analyses were conducted using the Student's test.

3. Results and discussion

3.1. Synthesis and characterization of PEG-SS-NH$_2$ and PEG-SS-BDP (PSSBDP)

A novel redox-responsive macro- photosensitizer PEG-SS-BDP for efficient PDT has been synthesized with PEG-SS-NH$_2$ and NHS-BDPBr conjunction (Fig. 1). Firstly, the active intermediate PEG-NPC was synthesized by replacing the hydroxyl end group of mPEG-OH (M_n = 2000 g/mol) with p-NPC, which could be inferred from the ^{1}H NMR spectra of PEG-NPC (Fig. 2a). The integration ratio of peak *a* (peak of methoxy protons of mPEG) to peak *d* + *f*, *c* + *e* (peaks of phenyl) is 3: 2: 2, indicating the successful activation of NPC. Then, PEG-SS-NH$_2$ was obtained by mixing the above intermediate with excess cystamine. The ^{1}H NMR spectra of PEG-SS-NH$_2$ in $CDCl_3$ is shown in Fig. 2b. The spectra supported the conversion of the NPC residue into cystamine. The disappearance of benzene peaks around 7.5 ppm and the existence of a peak at 2.91 ppm were assigned to the methylene protons of the cystamine moiety adjacent to the disulfide bond.

Finally, NHS-BDPBr we synthesized before has an ultrahigh singlet oxygen quantum yield (0.76) and its ^{1}H NMR spectra is shown in Fig. 2c. It was added to the end of redox-responsive PEG chain to obtain the amphiphilic macro- photosensitizer PSSBDP (^{1}H NMR spectra in Fig. 2d).

The successful conjunction of BDP and PEG-SS-NH$_2$ was also proved by the GPC curves of each polymer. In Fig. 3a, during the GPC measurements (DMF as fluent phase), novelty combination of a refractive index detector (RID) and a fluorescence detector (FLD) was performed in one system as series detectors. The FLD signals of PSSBDP appeared immediately after the RID ones, within about 10 s gap between the two detectors for series pipeline sake.

3.2. Redox-responsive behavior of PSSBDP

The amphiphilic macro-photosensitizer could be self-assembled into polymeric micelles as PSSBDP NPs by dialysis. The disulfide bond linkage (–SS–) between the hydrophobic BDP and hydrophilic PEG is expected to exhibit redox-sensitive properties. Because of the aggregation of hydrophobic BDP in aqueous, the agent release behavior of redox-responsive nanoparticles was conducted with 2% tween 80 (act as cosolvent) in buffer (PBS or 10 mM GSH in PBS as different conditions). The signal of BDP in the buffer was recorded by a fluoro-spectrophotometer to calculate the release content. The time-depend cumulative release percentages of BDP conjugated in PSSBDP micelles are plotted in Fig. 3b. The results show that without the existence of GSH, the accumulative release of BDP in the physiological buffer (pH = 7.4) reached about 12% within 12 h, with no further leakage observed till the end. In the presence of 10 mM GSH (imitating the intracellular environment, such as cytosol in cancer cells), the BDP release was distinctly enhanced and reached over 50% within 12 h and almost 70% after 48 h. The faster BDP release behavior from PSSBDP NPs under redox conditions was most attributed to the reduction-triggered cleavage of disulfide bonds in the block junction of the hydrophilic and hydrophobic segments (PEG and BDP), leads to rapid BDP release, as the micelles destabilized.

Qualitatively, the size distribution and morphology of PSSBDP NPs in different conditions (with or without GSH) were evaluated for redox-responsive characterization. The hydrodynamic size of these micelles in PBS is 114 nm in average by DLS in which the poly dispersion index (PDI) was 0.012 (Fig. 3c). The Zeta potential of the nanoparticles was detected as −8.12 mV (Fig. S2). While the size in TEM image is around 100 nm (Fig. 3e) and the slight difference is suggesting the existence of hydrophilic PEG corona in aqueous solution. The NPs with proper size can be also selectively accumulated in tumor tissue due to the enhanced permeability and retention (EPR) effect, which may improve the overall

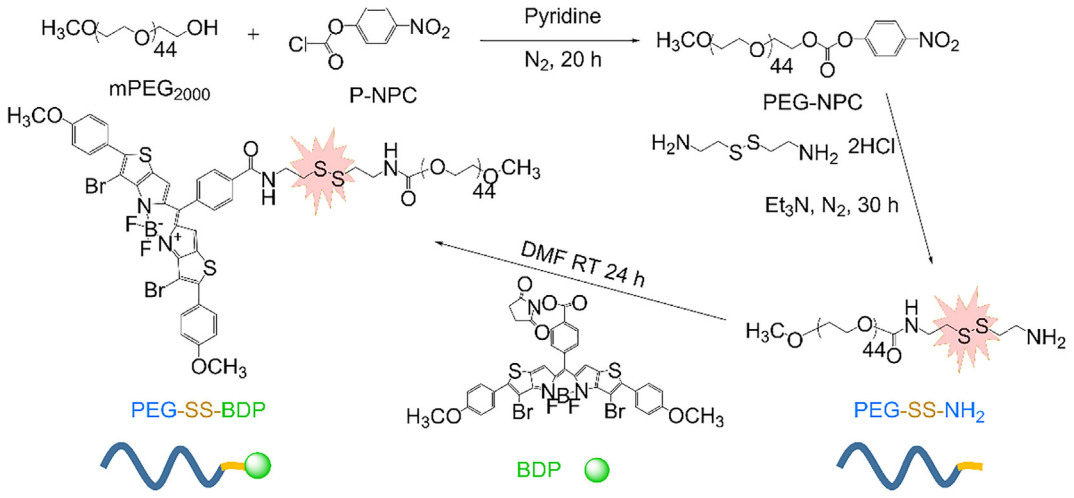

Fig. 1. Synthesis route of redox-responsive macro-photosensitizer PEG-SS-BDP.

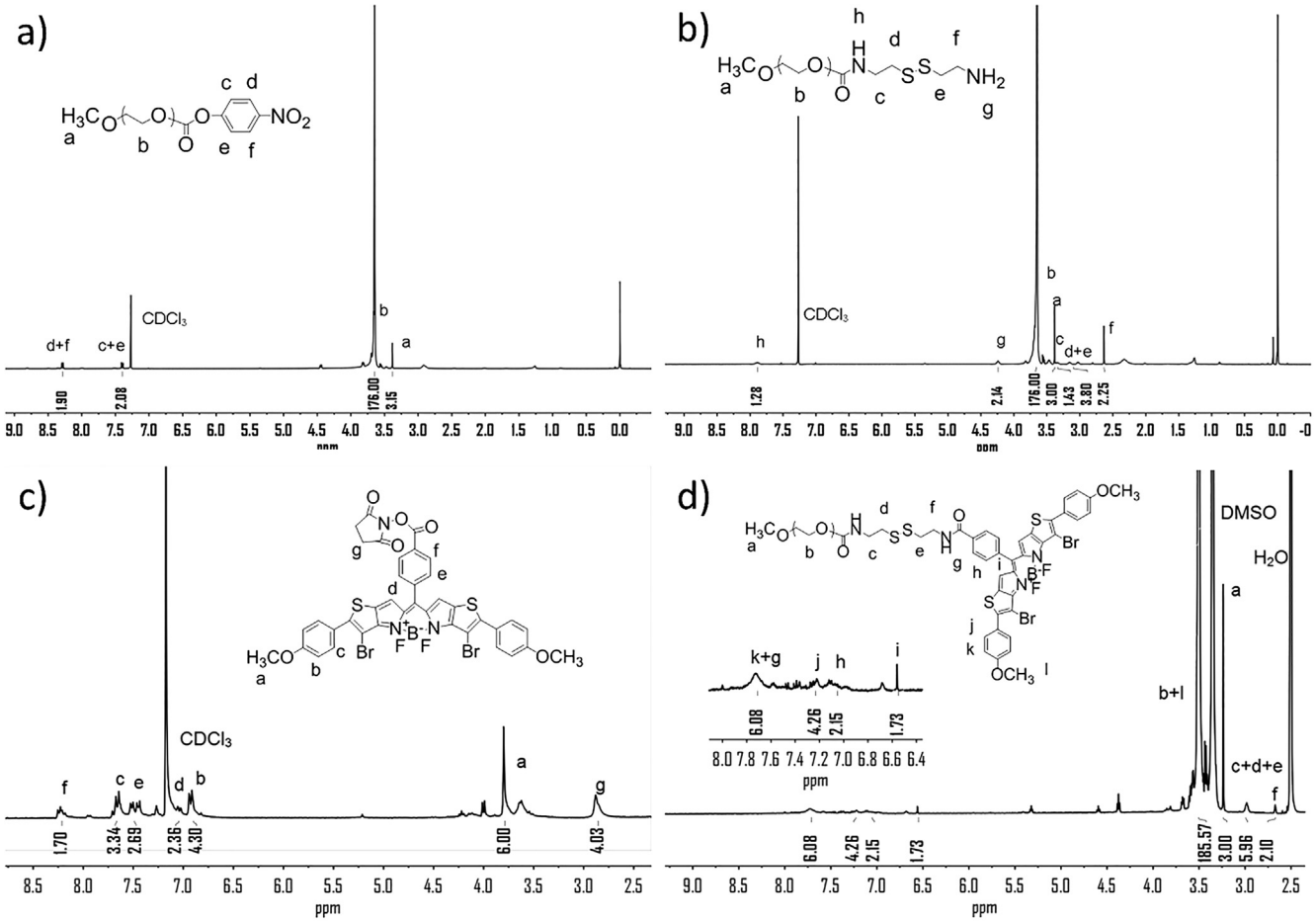

Fig. 2. ^{1}H NMR spectra of (a) PEG-NPC, (b) PEG-SS-NH_2, (c) high efficient photosensitizer NHS-BDPBr and (d) redox-responsive PEG-SS-BDP.

therapeutic efficacy *in vivo*. Besides, the nanoparticles PSSBDP showed colloidal stability with almost constant size distribution overtime post-preparation (6 h, 12 h, 24 h, 48 h, 72 h and 120 h, shown in Fig. S3). In 10 mM GSH solution, PSSBDP NPs seemed to be unstable as uniform micelles. There were mainly larger pieces detected by the DLS measurement (Fig. 3d). The size mainly increased which was likely caused by the splitting off of the intervening disulfide bonds, and this could rapidly lead to detachment of the hydrophilic PEG and aggregation of the hydrophobic BDP of the micelles. Meanwhile, spherical micelles were hardly found in TEM image (Fig. 3f).

3.3. Singlet oxygen detection by chemical trapping

Diphenylisobenzofuran (DPBF) is known as singlet oxygen scavenger and it traps the production of singlet oxygen through its oxidation. Singlet oxygen could interact with DPBF to yield 1, 2-dibenzoylbenzene, and the extent of DPBF-related photodegradation can be evaluated by measuring the decrease in the DPBF absorption peak at 414 nm (Fig. 4). As shown in Fig. 4a, it can be seen that the absorbance of DPBF reduces gradually under the irradiation. The PSSBDP mixture shown similar decrease rate as the standard MB (Fig. 4b). From Fig. 4c, the singlet oxygen quantum yield of the macro-photosensitizer PSSBDP was calculated as 0.55 compared with the MB (Φ_{Δ} = 0.57 in DCM).

3.4. Cytotoxicity evaluation

To assess the *in vitro* cytotoxicity of PSSBDP NPs, HepG2 (hepatocellular carcinoma cells from human) and EMT6 cells (mammary carcinoma cells from mouse) were employed to perform the 3-(4, 5-dimethylthiazol-2-yl)-2, 5-diphenyltetrazolium bromide (MTT) assays. As shown in Fig. 5a, without illumination (L−), the macro-photosensitizer micelles exhibited negligible toxicity after 24 h incubation. The maximum absorption peak of BDP is at about 675 nm. It is almost the longest wavelength as visible light which is closing to near infrared region. So we have chosen the 660 nm lamp for PDT performance experiments, which has limited penetration into solid tumors but suitable for the nanoparticles we prepared here. Upon a 660 nm laser output with power density of 20 mW/cm^2, gradient concentrations of PSSBDP (from 0.001 mg/mL to 0.005 mg/mL BDP) were added in the medium for cell incubation to check the PDT performance. PSSBDP NPs were noted for its highly toxic to HepG2 cells up to the concentration of 5 μg/mL BDP (cell viabilities < 30%). Similar cytotoxicity to EMT6 cells could be observed from the viability assays (Fig. 5b). Comparing with PBDP efficiency, PSSBDP shows higher cell toxicity (about 18% with 5 μg/mL BDP) which may be attributed to the release of BDP owing to the redox-responsive disulfide bond linkage.

Live/dead staining were conducted to support the MTT results with fluorescein diacetate (FDA) and propidium iodide (PI). From the fluorescence images excited by corresponding wavelength, in which the green signal (FDA) represented alive cells and red (PI) for dead ones, we could check the good biocompatibility of PSSBDP itself without illumination (Fig. 6, L−). While with NIR irradiation, dead cells were obviously existed in both HepG2 and EMT6 groups (Fig. 6, L+). Most cells were killed with 20 mW/cm^2 which was accord with the MTT result, suggesting the forceful damage of PSSBDP NPs to different cell lines even with such low-power density of NIR light.

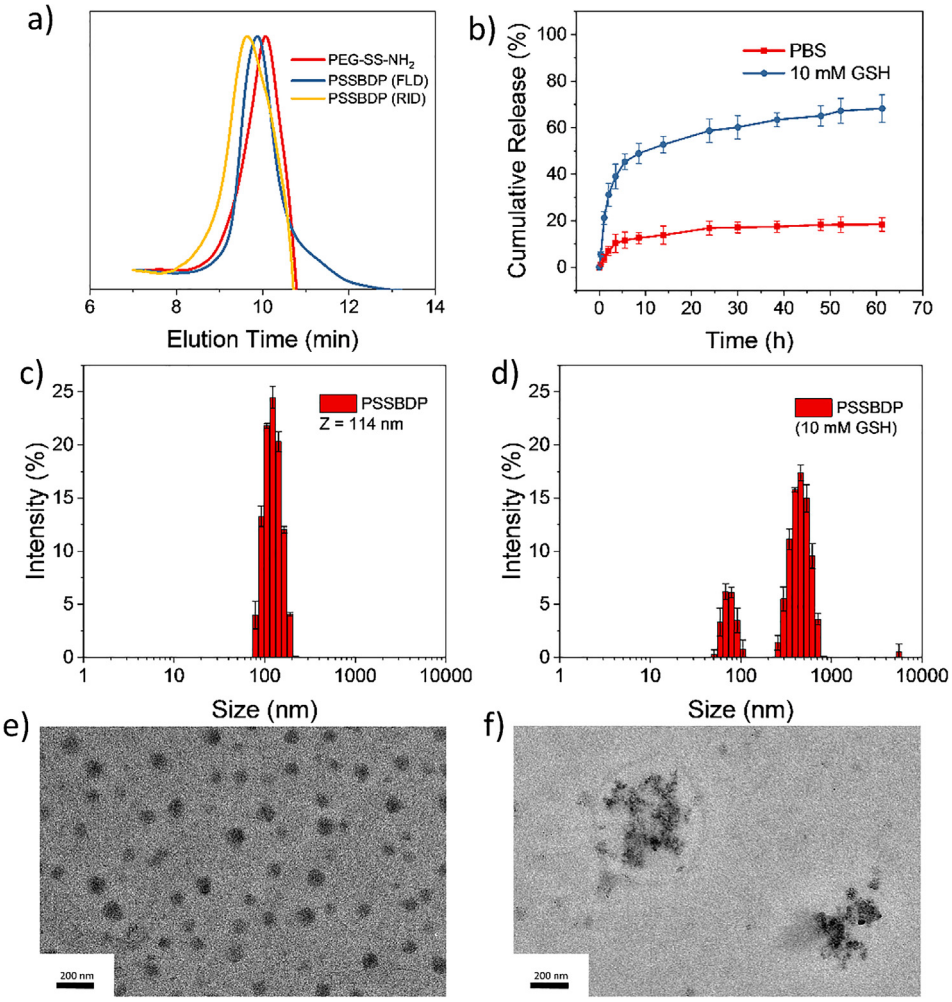

Fig. 3. (a) GPC data of PEG-SS-NH_2 and PSSBDP with a refractive index detector and a fluorescence detector. (b) Cumulative release of BDP in PBS or 10 mW GSH solution (both with 2% tween 80). Hydrodynamic diameter and corresponding TEM images of PEG-SS-BDP NPs in PBS (c, e) or with 10 mM GSH (d, f).

3.5. Cellular internalization

To further demonstrate the cellular uptake behavior of PSSBDP micelles, at 24 h post incubation, 4,6-diamino-2-phenyl indole (DAPI) was used to stain the nucleus of cells including the HepG2 and EMT6 cells. As shown in Fig. 7a, after 25 min of DAPI incubation with HepG2 cells, the red fluorescence intensity of BDP was distinctly observed well-dispersing throughout the cytoplasm while the blue signal represented DAPI-stained nucleus. The favorable dispersity of BDP is potential for effective photodynamic therapy. Similar intracellular fluorescence signals of PSSBDP NPs were found in EMT6 cells (Fig. 7b).

3.6. Biodistribution and accumulation of PSSBDP NPs in vivo

The NIR imaging ability of PSSBDP NPs was strongly confirmed *in vitro*. According to literatures, nanoparticles with proper size have the enhanced permeability and retention (EPR) effect because of the loose blood vessels in tumor area [44]. To EMT6 tumor-bearing mice divided randomly, PBS, free BDP molecules (in 1% DMSO) and PSSBDP NPs (BDP at the same concentration of 5 mg/kg mice bodyweight) were injected *via* tail vein for blood circulation. The fluorescence images of mice in each group were taken by a Xenogen IVIS® Lumina system at predominant time points (2 h, 6 h, 12 h, 24 h and 48 h, Fig. 8a). After

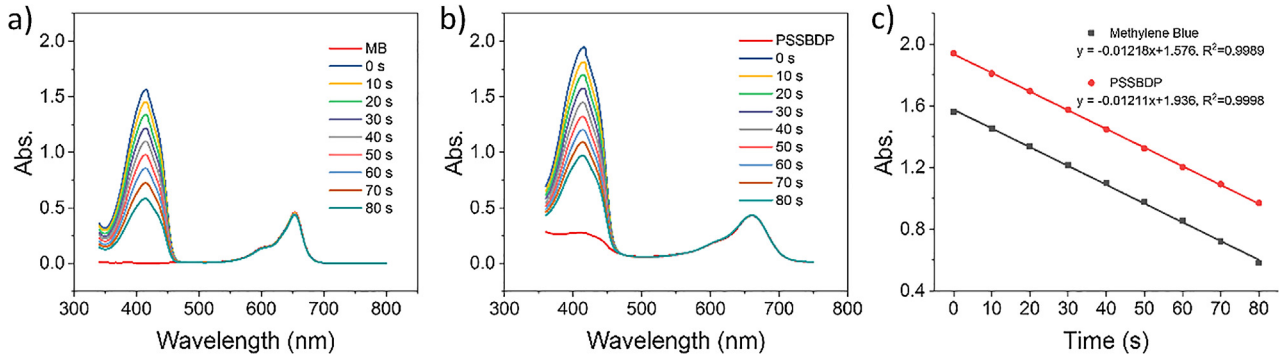

Fig. 4. Changes in the DPBF absorbance spectra in the presence of MB (a), PSSBDP (b) and their plots of absorbance decrease rate (c) at 414 nm under irradiation.

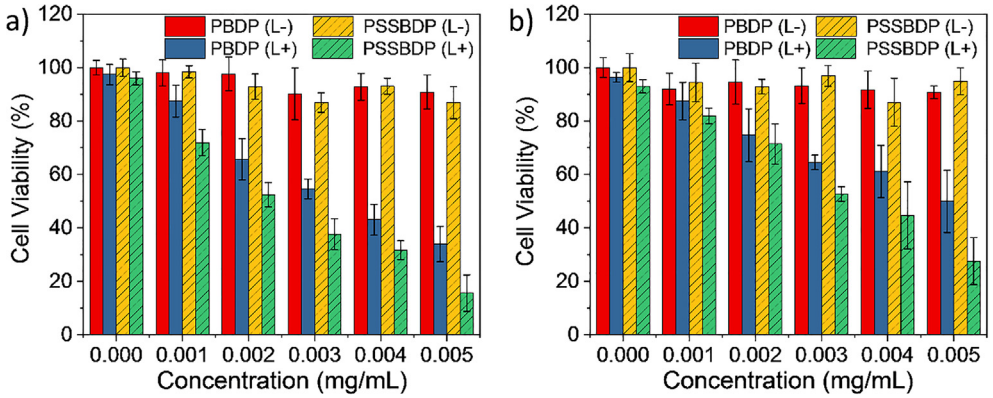

Fig. 5. Dark toxicity (L−) and phototoxicity (L+) of non-responsive PBDP NPs and redox-responsive PSSBDP NPs toward HepG2 (a) and EMT6 (b) cells for 24 h, analyzed by MTT assay.

treatment with PSSBDP NPs, the fluorescence signal of photosensitizer was obviously accumulated at the tumor site and it regularly increased at the first 12 h after injection (Fig. 8b). Besides, its average fluorescence intensity in tumors was much stronger than that in other organs. Subsequently, the fluorescence signal of photosensitizer has gradually declined without further treatment. By contrast, the strongest fluorescence signal of photosensitizer has arisen at the first 6 h post-injection at tumor site of mice treated with free BDP molecules, then it rapidly decreased (black line in Fig. 8b). After 48 h post-injection, mice in each group were sacrificed. Main organs and tumors were collected for *ex vivo* fluorescence performance. As shown in Fig. 8c, stronger BDP fluorescence signal in tumor was noticed in PSSBDP NPs group than that in free BDP groups (about 5-fold). And the analysis of total radiant efficiency in tumor and main organs was shown in Fig. 8d.

We suggested that the EPR effect could provide the much better accumulation at tumor site of PBDPI NPs with proper size (about

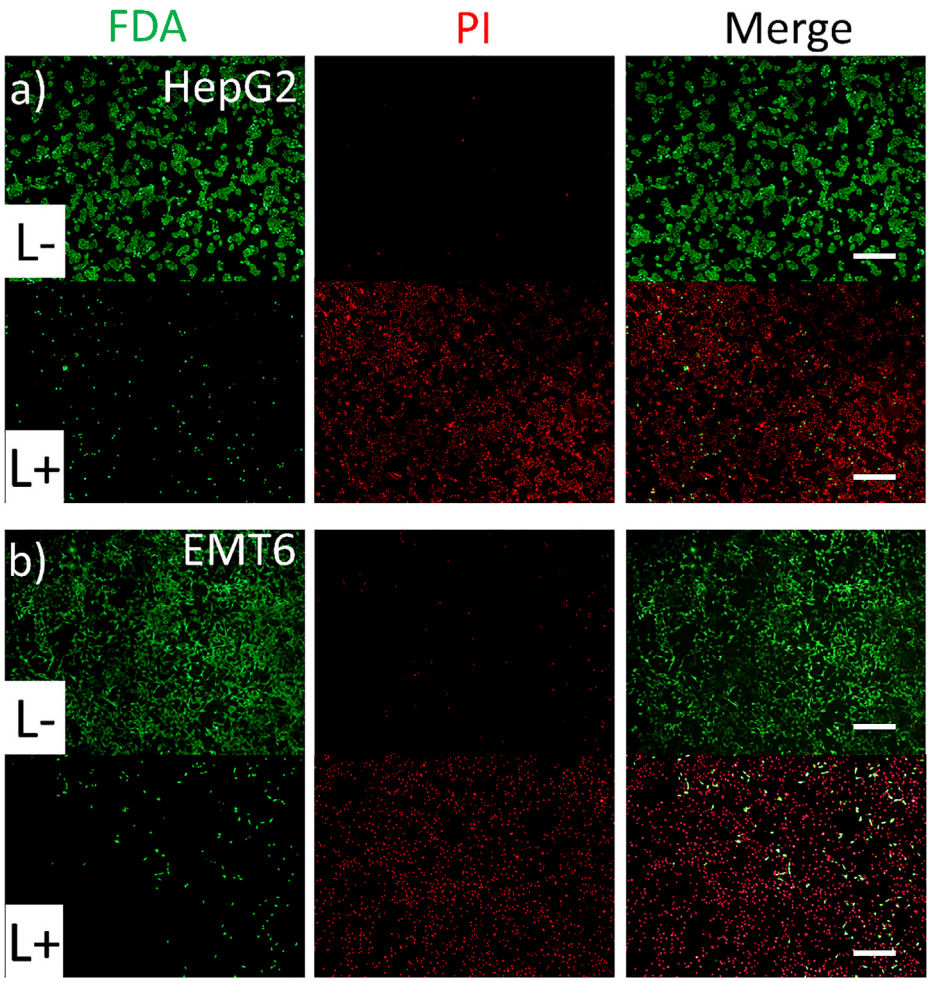

Fig. 6. Photodamage detection by fluorescence microscope using fluorescent probes (live/dead staining with FDA and PI). Green fluorescence of live cells (FDA) and red fluorescence of dead cells (PI). Scale bar = 200 μm. (For interpretation of the references to colour in this figure legend, the reader is referred to the web version of this article.)

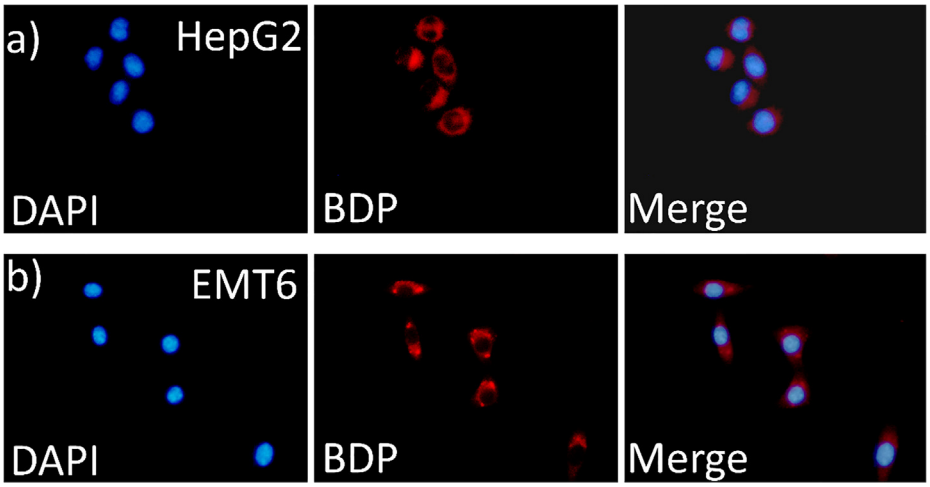

Fig. 7. Cellular uptake and intracellular localization of PSSBDP NPs incubated with HepG2 (a) and EMT6 (b) cancer cells for 24 h, respectively.

110 nm). The free BDP molecules could be quickly cleaned up during the blood circulation. Moreover, the hemolytic potential of the PSSBDP NPs has been assessed by incubating the NPs with red blood cells. After centrifugation, red blood cells still located at the bottom indicating no damage to erythrocyte (Fig. S4). Generally speaking, the redox-responsive macro photosensitizer PSSBDP NPs we prepared showed the possibility for prolonged blood circulation and precise tumor accumulation.

3.7. *In vivo* tumor suppression by PSSBDP NPs PDT

Tumor growth inhibition with the PSSBDP NPs formulation was performed *in vivo* in mice with EMT6 tumor-bearing on both sides. The mice were treated with free BDP molecules, PBDP NPs (prepared according to former research) and the redox-responsive PSSBDP NPs at a BDP dose of 5 mg per kg of body weight while PBS was used as control. The injection was conducted only twice at the beginning (Fig. 9a). Illumination with a 660 nm laser (25 mW/cm^2, 20 min) was given just on

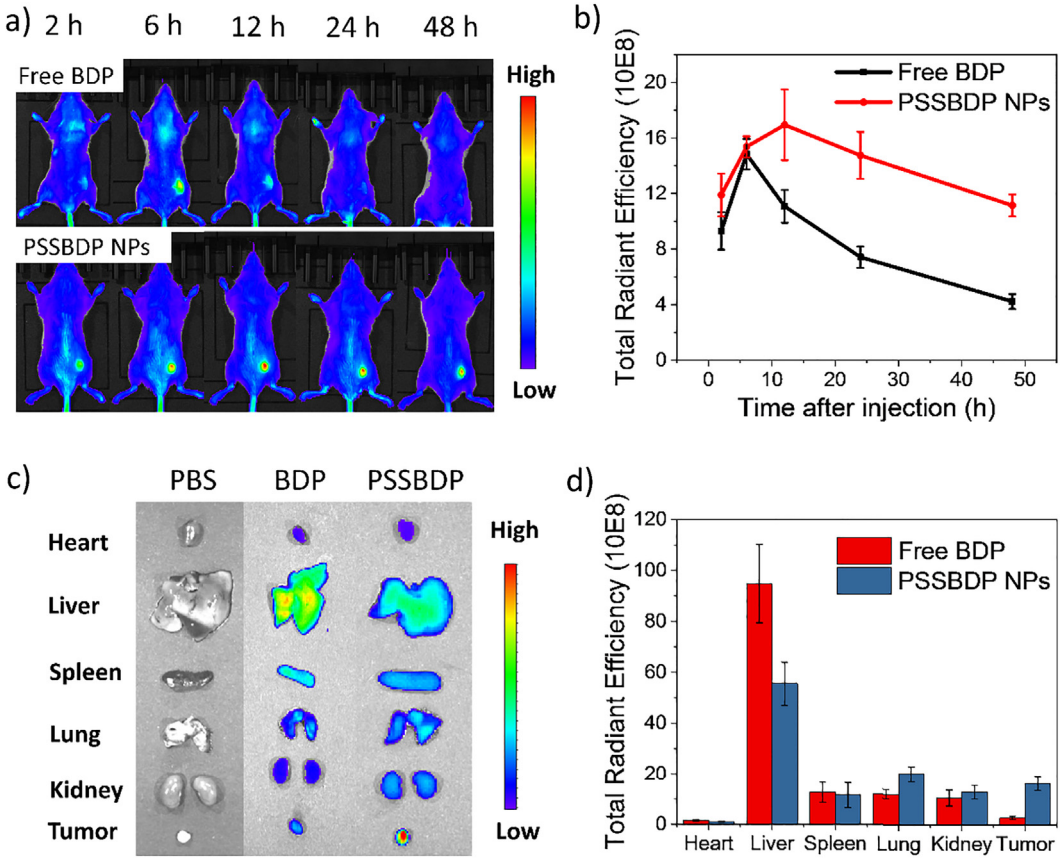

Fig. 8. (a) *In vivo* time-dependent NIR (675 nm) excited fluorescence imaging of EMT6 tumor-bearing mice after intravenous injection of free BDP and PSSBDP NPs. (b) Quantification of total radiant efficiency of free BDP molecule and PSSBDP NPs treated mice in the tumor site. (C) *Ex vivo* fluorescence images of major organs and tumors of mice after intravenous injection of PBS, free BDP molecules and PSSBDP NPs post 48 h-injection. (D) Quantification of total radiant efficiency of main organs and tumors.

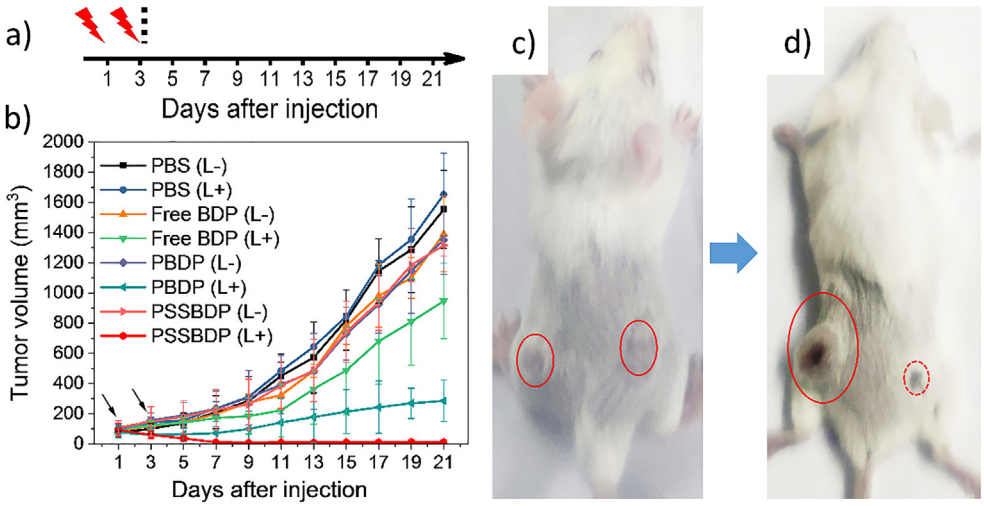

Fig. 9. *In vivo* study of PDT efficiency after administration. (a) Injection and illumination time points on the first and third day. (d) Tumor volume change of each group during the treatment, black arrows indicate injection for only twice. Blackboard arrows represent injection and illumination. Digital photographs of mice prepared for injection (c) and mice after 21 days post treatment with PSSBDP NPs (d).

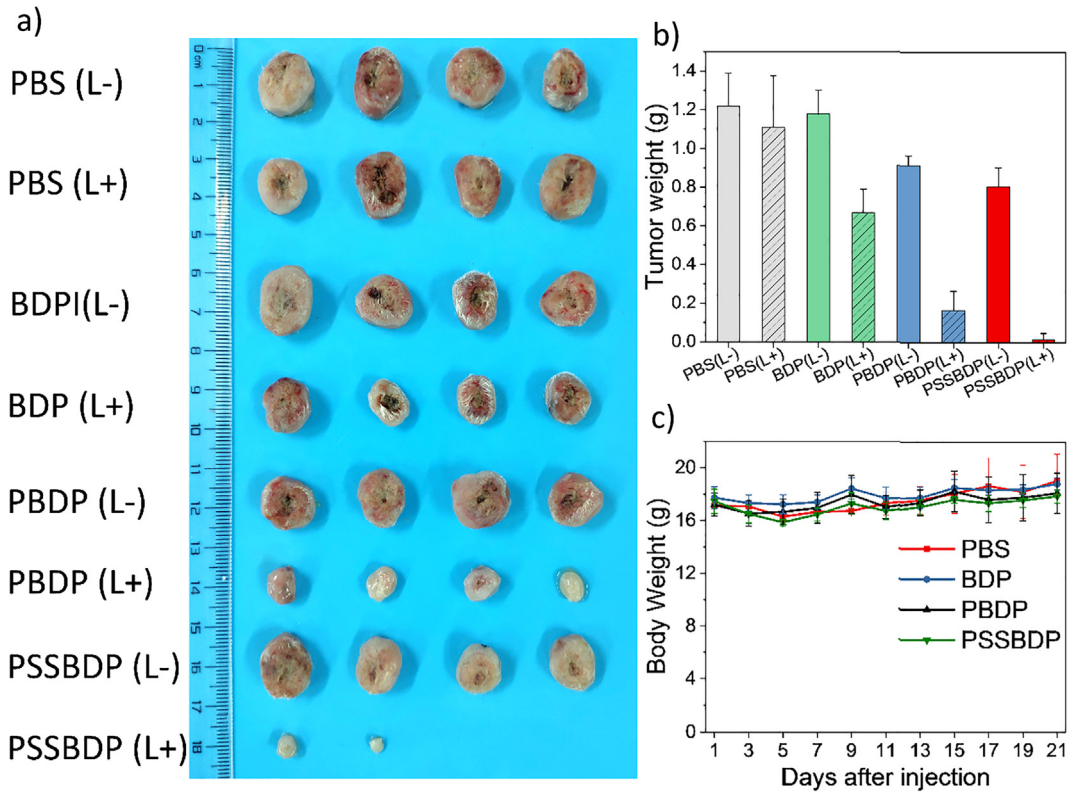

Fig. 10. (a) Images of the tumors after the 21 days treatment with PBS, free BDP, non-responsive PBDP NPs and redox-responsive PSSBDP NPs, all groups were treated with (L+) or without (L−) illumination. (b) Tumor wet weights in different groups (in panel a) after 21 days treatment. (c) Body weight records of the mice in different groups within 21 days treatment. The data are shown as mean ± SD (n = 4).

the right side tumors at 12 h post-injection, which was inspired by the *in vivo* bioimaging results. Though the penetration ability of 660 nm laser is limited, it is suitable for the photosensitizer and subcutaneous tumors we used here. To quantitatively evaluate the photodynamic therapeutic efficacy in different groups, the tumor growth rate of the EMT6 tumor-bearing mice was also examined every other day for 21 days. As shown in Fig. 9b, when the mice were treated with PBS only, the growth with or without the NIR laser irradiation tumor was hardly restrained and found to have an average volume of 1600 mm^3 at 21st day post-treatment. The tumors on the left treated with free BDP, PBDP NPs or PSSBDP NPs (without illumination) showed similar growth as the PBS group, indicating the non-toxicity property of the photosensitizer itself without illumination. After 21 days, for free BDP (with illumination, L+) treated mice, the average volume of the tumor was about 950 mm^3, which is 59.4% of the volume of the tumor that in PBS group. It could be inferred that free BDP molecules displayed limited inhibition on tumor growth mainly due to its poor accumulation at tumor site. PBDP NPs showed enhanced suppression. In the case of PBDP NPs (L+) treated mice, although tumor inhibition was seen at the necrotic scar site in the first five days, then the tumor in several mice began to grow rapidly around the scar. The final average volume of tumors in PBDP (L+) group was about 290 mm^3, decreased 81.9% of the tumor volume recorded for the PBS with illumination treated group. Meanwhile, the redox-responsive PSSBDP NPs showed the strongest suppression on tumor growth that tumors were completely inhibited and no reoccurrence was noticed, in which group tumors can be cured even without

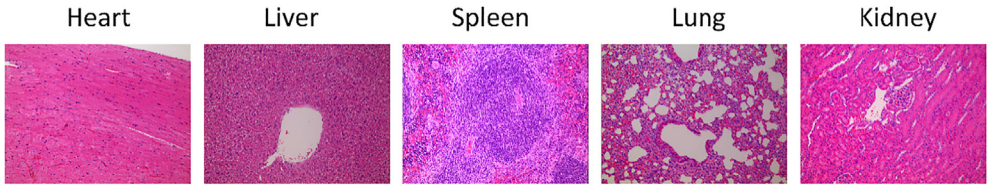

Fig. 11. H&E stained images of major organs (magnification: ×200). After PSSBDP injection without laser treatment, the mice were sacrificed and no noticeable abnormality was observed in the heart, liver, spleen, lung and kidney.

wounds (Fig. 9d). This noticeable inhibition in tumor growth, which is remarkably more effective than free BDP/irradiation or PBDP/irradiation treatment, may be attributed to the long tumor retention time and redox-responsive agent release behavior of the PSSBDP NPs.

Then the mice were sacrificed with tumors collection for digital photograph (Fig. 10a) and wet weight record (Fig. 10b). The image of tumor and wet weight analysis were accord with the tumor growth, indicating the high PDT efficiency of PSSBDP NPs. Body weight reduction was concerned for treatment-induced toxicity. Clearly, No noteworthy weight loss was observed, suggesting that the PDT effects of the PSSBDP NPs was not triggered by the toxicity of nanoparticles (Fig. 10c).

Histology experiments was carried out to further investigate the potential toxic side effects of the nanoparticles. The mice treated with PSSBDP (without illumination) were sacrificed and the major organs of the mice were removed and subjected to H&E staining. No abnormality was observed in the heart, liver, spleen, lung and kidney tissue slices (Fig. 11). These data showed that the redo-responsive PSSBDP nanoparticles for PDT did not cause significant adverse effects *in vivo*. Overall, these results above demonstrate that the PDT treatment of tumors using the combination of PSSBDP NPs and NIR laser irradiation can induce remarkable anticancer efficacy with negligible side effects.

4. Conclusion

In summary, a simple method has been developed to prepare amphiphilic polymeric pro-PS and assembling redox-responsive polymeric micelles by introducing the disulfide bonds, which connected the hydrophobic NIR photosensitizer BDP with hydrophilic PEG block. The suitable size of PEG-SS-BDP (PSSBDP) was found to perform excellently for cellular uptake and tumor accumulation. Once the pro-PS NPs accumulates at the tumor site by the EPR effect, it shows outstanding NIR bioimaging ability. After internalized by cancer cells, the PEG shell can be removed and then trigger the BDP release by excess intracellular GSH. Spread of the BDP ships the singlet oxygen closing to the organelle to ensure the inducing cell apoptosis. With only twice injection and illumination at the beginning, the redox-responsive PDT agent shows showed higher therapeutic efficacy to EMT6 tumor-bearing mice, which could even suppress the tumor to disappear with scar. These results suggested that the innovative redox-responsive PSSBDP carrier might provide new prospects for controlled photosensitizer release in imaging-guided photodynamic therapy.

Conflicts of interest

There are no conflicts to declare.

Acknowledgements

This work is supported by the National Natural Science Foundation of China, China (No. 51373162 and 51673180).

Appendix A. Supplementary material

Supplementary data to this article can be found online at https://doi.org/10.1016/j.ejpb.2018.12.006.

References

[1] D.E.J.G.J. Dolmans, D. Fukumura, R.K. Jain, Photodynamic therapy for cancer, Nat. Rev. Cancer 3 (2003) 380–387.
[2] H. Abrahamse, M.R. Hamblin, New photosensitizers for photodynamic therapy, Biochem. J. 473 (2016) 347–364.
[3] R. Bonnett, Photosensitizers of the porphyrin and phthalocyanine series for photodynamic therapy, Chem. Soc. Rev. 24 (1995) 19–33.
[4] X.S. Li, S. Kolemen, J. Yoon, E.U. Akkaya, Activatable photosensitizers: agents for selective photodynamic therapy, Adv. Funct. Mater. 27 (2017).
[5] J.P. Celli, B.Q. Spring, I. Rizvi, C.L. Evans, K.S. Samkoe, S. Verma, B.W. Pogue, T. Hasan, Imaging and photodynamic therapy: mechanisms, monitoring, and optimization, Chem. Rev. 110 (2010) 2795–2838.
[6] M.C. DeRosa, R.J. Crutchley, Photosensitized singlet oxygen and its applications, Coordin. Chem. Rev. 233 (2002) 351–371.
[7] M. Redza-Dutordoir, D.A. Averill-Bates, Activation of apoptosis signalling pathways by reactive oxygen species, Bba-Mol. Cell. Res. 1863 (2016) 2977–2992.
[8] H.U. Simon, A. Haj-Yehia, F. Levi-Schaffer, Role of reactive oxygen species (ROS) in apoptosis induction, Apoptosis 5 (2000) 415–418.
[9] A. Kamkaew, S.H. Lim, H.B. Lee, L.V. Kiew, L.Y. Chung, K. Burgess, BODIPY dyes in photodynamic therapy, Chem. Soc. Rev. 42 (2013) 77–88.
[10] S.H. Lim, C. Thivierge, P. Nowak-Sliwinska, J.Y. Han, H. van den Bergh, G. Wagnieres, K. Burgess, H.B. Lee, In vitro and in vivo photocytotoxicity of boron dipyrromethene derivatives for photodynamic therapy, J. Med. Chem. 53 (2010) 2865–2874.
[11] S.G. Awuah, Y. You, Boron dipyrromethene (BODIPY)-based photosensitizers for photodynamic therapy, Rsc Adv. 2 (2012) 11169–11183.
[12] T. Yogo, Y. Urano, Y. Ishitsuka, F. Maniwa, T. Nagano, Highly efficient and photostable photosensitizer based on BODIPY chromophore, J. Am. Chem. Soc. 127 (2005) 12162–12163.
[13] W.L. Sheng, J.E. Cui, Z. Ruan, L.F. Yan, Q.H. Wu, C.J. Yu, Y. Wei, E.H. Hao, L.J. Jiao, [a]-Phenanthrene-fused BF2 azadipyrromethene (AzaBODIPY) dyes as bright near-infrared fluorophores, J. Org. Chem. 82 (2017) 10341–10349.
[14] A. Loudet, K. Burgess, BODIPY dyes and their derivatives: Syntheses and spectroscopic properties, Chem. Rev. 107 (2007) 4891–4932.
[15] P. Yuan, Z. Ruan, W. Jiang, L. Liu, J.X. Dou, T.W. Li, L.F. Yan, Oxygen self-sufficient fluorinated polypeptide nanoparticles for NIR imaging-guided enhanced photodynamic therapy, J. Mater. Chem. B 6 (2018) 2323–2331.
[16] J.H. Zou, Z.H. Yin, K.K. Ding, Q.Y. Tang, J.W. Li, W.L. Si, J.J. Shao, Q. Zhang, W. Huang, X.C. Dong, BODIPY derivatives for photodynamic therapy: influence of configuration versus heavy atom effect, Acs Appl. Mater. Inter. 9 (2017) 32475–32481.
[17] I.S. Turan, D. Yildiz, A. Turksoy, G. Gunaydin, E.U. Akkaya, A Bifunctional photosensitizer for enhanced fractional photodynamic therapy: singlet oxygen generation in the presence and absence of light, Angew. Chem. Int. Ed. 55 (2016) 2875–2878.
[18] X.F. Zhang, BODIPY photosensitizers based on PET and heavy atom effect: A comparative study on the efficient formation of excited triplet state and singlet oxygen in BODIPY dimers and monomers, J. Photoch. Photobio. A 355 (2018) 431–443.
[19] D.J. Lee, Y.S. Youn, E.S. Lee, Photodynamic tumor therapy of nanoparticles with chlorin e6 sown in poly(ethylene glycol) forester, J. Mater. Chem. B 3 (2015) 4690–4697.
[20] L. Liu, L.Y. Fu, T.T. Jing, Z. Ruan, L.F. Yang, pH-triggered polypeptides nanoparticles for efficient BODIPY imaging-guided near infrared photodynamic therapy, Acs Appl. Mater. Inter. 8 (2016) 8980–8990.
[21] Y.N. Konan, R. Gurny, E. Allemann, State of the art in the delivery of photosensitizers for photodynamic therapy, J. Photoch. Photobio. B 66 (2002) 89–106.
[22] S.S. Lucky, K.C. Soo, Y. Zhang, Nanoparticles in photodynamic therapy, Chem. Rev. 115 (2015) 1990–2042.
[23] D.K. Chatterjee, L.S. Fong, Y. Zhang, Nanoparticles in photodynamic therapy: An emerging paradigm, Adv. Drug Deliver. Rev. 60 (2008) 1627–1637.
[24] S. Dufort, L. Sancey, J.L. Coll, Physico-chemical parameters that govern nanoparticles fate also dictate rules for their molecular evolution, Adv. Drug Deliver. Rev. 64 (2012) 179–189.
[25] J. Fang, H. Nakamura, H. Maeda, The EPR effect: Unique features of tumor blood vessels for drug delivery, factors involved, and limitations and augmentation of the effect, Adv. Drug Deliver. Rev. 63 (2011) 136–151.
[26] D. Peer, J.M. Karp, S. Hong, O.C. FaroKHzad, R. Margalit, R. Langer, Nanocarriers as an emerging platform for cancer therapy, Nat. Nanotechnol. 2 (2007) 751–760.
[27] X.Z. Ai, J. Mu, B.G. Xing, Recent advances of light-mediated theranostics, Theranostics 6 (2016) 2439–2457.
[28] C. Wang, H.Q. Tao, L. Cheng, Z. Liu, Near-infrared light induced in vivo photodynamic therapy of cancer based on upconversion nanoparticles, Biomaterials 32

(2011) 6145–6154.
[29] S.G. Awuah, J. Polreis, V. Biradar, Y. You, Singlet oxygen generation by novel NIR BODIPY dyes, Org. Lett. 13 (2011) 3884–3887.
[30] Z. Ruan, Y.Y. Zhao, P. Yuan, L. Liu, Y.C. Wang, L.F. Yan, PEG conjugated BODIPY-Br-2 as macrophotosensitizer for efficient imaging-guided photodynamic therapy, J. Mater. Chem. B 6 (2018) 753–762.
[31] C.G. Alves, R. Lima-Sousa, D. de Melo-Diogo, R.O. Louro, I.J. Correia, IR780 based nanomaterials for cancer imaging and photothermal, photodynamic and combinatorial therapies, Int. J. Pharmaceut. 542 (2018) 164–175.
[32] S. Hatz, L. Poulsen, P.R. Ogilby, Time-resolved singlet oxygen phosphorescence measurements from photosensitized experiments in single cells: Effects of oxygen diffusion and oxygen concentration, Photochem. Photobiol. 84 (2008) 1284–1290.
[33] Z. Ruan, L. Liu, W. Jiang, S.Y. Li, Y.C. Wang, L.F. Yan, NIR imaging-guided combined photodynamic therapy and chemotherapy by a pH-responsive amphiphilic polypeptide prodrug, Biomater. Sci. 5 (2017) 313–321.
[34] X.J. Jiang, J.T.F. Lau, Q. Wang, D.K.P. Ng, P.C. Lo, pH- and thiol-responsive BODIPY-based photosensitizers for targeted photodynamic therapy, Chem-Eur J 22 (2016) 8273–8281.
[35] L.B. Meng, W.Y. Zhang, D.Q. Li, Y. Li, X.Y. Hu, L.Y. Wang, G.G. Licd, pH-Responsive supramolecular vesicles assembled by water-soluble pillar[5]arene and a BODIPY photosensitizer for chemo-photodynamic dual therapy, Chem. Commun. 51 (2015) 14381–14384.
[36] M. Huo, J.Y. Yuan, L. Tao, Y. Wei, Redox-responsive polymers for drug delivery: from molecular design to applications (vol 5, pg 1519, Polym. Chem. 5 (2014) (2014) 5183–5183.
[37] R. Cheng, F. Feng, F.H. Meng, C. Deng, J. Feijen, Z.Y. Zhong, Glutathione-responsive nano-vehicles as a promising platform for targeted intracellular drug and gene delivery, J. Control. Release 152 (2011) 2–12.
[38] R.L. McCarley, Redox-responsive delivery systems, Annu. Rev. Anal. Chem. 5 (2012) 391–411.
[39] P. Kuppusamy, H.Q. Li, G. Ilangovan, A.J. Cardounel, J.L. Zweier, K. Yamada, M.C. Krishna, J.B. Mitchell, Noninvasive imaging of tumor redox status and its modification by tissue glutathione levels, Cancer Res. 62 (2002) 307–312.
[40] T.T. Jing, L.Y. Fu, L. Liu, L.F. Yan, A reduction-responsive polypeptide nanogel encapsulating NIR photosensitizer for imaging guided photodynamic therapy, Polym. Chem. 7 (2016) 951–957.
[41] Y. Yan, Y.J. Wang, J.K. Heath, E.C. Nice, F. Caruso, Cellular association and cargo release of redox-responsive polymer capsules mediated by exofacial thiols, Adv. Mater. 23 (2011) 3916-+.
[42] J. Zhang, F. Yang, H. Shen, D.C. Wu, Controlled formation of microgels/nanogels from a disulfide-linked core/shell hyperbranched polymer, Acs Macro Lett. 1 (2012) 1295–1299.
[43] J. Xia, L.W. Zhang, M. Qian, Y.M. Bao, J.Y. Wang, Y.C. Li, Specific light-up pullulan-based nanoparticles with reduction-triggered emission and activatable photoactivity for the imaging and photodynamic killing of cancer cells, J. Colloid Interf. Sci. 498 (2017) 170–181.
[44] A. Nel, E. Ruoslahti, H. Meng, New insights into “permeability” as in the enhanced permeability and retention effect of cancer nanotherapeutics, Acs Nano 11 (2017) 9567–9569.